Kunwar, Puskal; Hassinen, Jukka; Bautista, Godofredo; Ras, Robin; Toivonen, Juha

Direct Laser Writing of Photostable Fluorescent Silver Nanoclusters in Polymer Films

Published in:
ACS Nano

DOI:
10.1021/nn5059503

Published: 01/11/2014

Document Version
Peer reviewed version

Please cite the original version:
Kunwar, P., Hassinen, J., Bautista, G., Ras, R. H. A., & Toivonen, J. (2014). Direct Laser Writing of Photostable Fluorescent Silver Nanoclusters in Polymer Films. ACS Nano, 8(11), 11165-11171.
https://doi.org/10.1021/nn5059503

Direct Laser Writing of Photostable Fluorescent Silver Nanoclusters in Polymer Films

Puskal Kunwar[†], *Jukka Hassinen*[‡], *Godofredo Bautista*[†], *Robin H. A. Ras*[‡,*], *and Juha Toivonen*[†,*]

†Department of Physics, Tampere University of Technology, P.O. Box 692, FI-33101 Tampere, Finland

‡Department of Applied Physics, Aalto University (Helsinki University of Technology), P.O. Box 11000, FI-02150 Espoo, Finland

* email: robin.ras@aalto.fi, juha.toivonen@tut.fi

ABSTRACT

Metal nanoclusters consist of a few to few hundreds of atoms, and exhibit attractive molecular properties such as ultrasmall size, discrete energy levels and strong fluorescence. Although patterning of these clusters down to the microscale or nanoscale could lead to applications such as high-density data storage, it has been reported only for inorganic matrices. Here we demonstrate the first submicron-scale mask-free patterning of fluorescent silver nanoclusters in an organic matrix. The nanoclusters were produced by direct laser writing in poly(methacrylic acid) thin films, and exhibit a broadband emission at visible wavelengths with photostability that is superior to Rhodamine 6G dye. This fabrication method could open new opportunities for applications in nanophotonics like imaging, labeling, and metal ion sensing. We foresee that this method can be further applied to prepare other metal nanoclusters embedded in compositionally different polymer matrices.

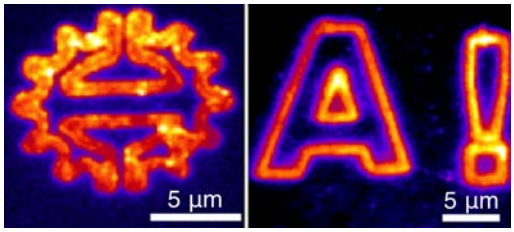

KEYWORDS

Optical lithography, metal nanoclusters, photoluminescence, photobleaching, photostability, polymer

Metal nanoclusters encompass a new class of luminescent nanomaterials with metal cores consisting of a couple of atoms up to nuclearities of few hundreds, therefore acting as an intermediate state between isolated metal atoms and nanoparticles.[1,2] They are receiving increasing interest because of their significantly different optical, electrical and chemical properties compared to their larger counterparts.[3] For ultrasmall nanoclusters, the continuous density of states breaks up into discrete energy levels leading to molecule-like properties such

as strong fluorescence. Due to their intrinsic fluorescence, metal nanoclusters have been proposed for applications such as data storage, biological labeling and detection of metal ions, nucleic acids and proteins.[4,5] The fluorescence is typically observed as broadband emission in the visible range and often displays characteristics of inhomogeneous broadening.[6] The presence of strong fluorescence combined with photostability, large Stokes shift and absence of localized surface plasmon resonance peak in their extinction spectrum differentiates such metal nanoclusters from their nanoparticle counterparts.[2,3]

Silver nanoclusters are often difficult to synthesize in aqueous solution, as they tend to aggregate and form larger particles. Generally, the formation of silver nanoclusters can be achieved by reducing silver ions to a zero-valent state and stabilizing the as-generated nanoclusters simultaneously to prevent further growth. Conventionally, reduction of silver ions can be accomplished by using chemical reductants,[7,8] electrochemistry[9] or by irradiating Ag^+ solutions with gamma-rays,[10] UV,[11] visible light,[12,13] microwaves[14] or ultrasound.[15] Stabilization can be attained by reducing the silver ions in the presence of stabilizer molecules, such as polymers, dendrimers or deoxyribonucleic acid (DNA).[2,3] Alternatively, photostable silver nanoclusters can be produced in inorganic solids such as glasses[16,17] and zeolites[18] by using femtosecond direct laser writing (DLW).

The development of femtosecond laser has been recognized in 1999 with the Nobel Prize in Chemistry.[19] The key features of the femtosecond laser are its exceptionally high power density and precise delivery of pulse energies in time and space. Because of these salient features, the femtosecond laser is useful in multi-photon DLW, where a tightly focused laser beam is scanned in a photosensitive material to fabricate three-dimensional (3D) structures.[20,21,22] Such nanofabricated materials have been widely used for many applications such as photonic crystals, metamaterials, microfluidics and biomedical implants.[21] Furthermore, there has been a continuous effort in creating 3D,[23] fluorescent[24] and metal[25]

58 microstructures using this technique. Clearly, this two-photon-based absorption technique
59 outperforms other optical lithographic techniques in terms of 3D spatial resolution and
60 flexibility.

61 Poly(methacrylic acid) (PMAA) is an excellent stabilizing agent in generating brightly
62 fluorescent silver nanoclusters.[12,13] Broadband visible light irradiation of an aqueous solution
63 of PMAA and $AgNO_3$ has been shown to form $(Ag)_n$@PMAA nanoclusters that emit red light
64 with a quantum yield of 18.6%.[12] However, this procedure is limited to the formation of
65 nanoclusters in solution. Furthermore, illuminating a solid thin film of PMAA containing
66 silver nitrate with similar broadband visible light leads to the formation of large silver
67 particles that are non-fluorescent. In addition, these nanoclusters generally lose their
68 fluorescence properties when the cluster-containing aqueous solution is dried or spin coated.

69 In this article, we demonstrate the submicron-scale fabrication of fluorescent
70 microstructures by stabilizing silver nanoclusters in a polymer film using DLW. We study the
71 optical properties of the nanoclusters and investigate the DLW-induced structural changes in
72 the polymer films. We found that the nanoclusters possess a broadband emission in the visible
73 range, and show photostability that is superior to the well-known Rhodamine 6G dye.

RESULTS AND DISCUSSION

Written structures are fluorescent. Figure 1a depicts the bright field image of line arrays fabricated by DLW with laser intensity (I_{dlw}) of 80 GW/m^2, wavelength (λ_{dlw}) of 780 nm and scanning speed of 10 μm/s in 50% Ag@PMAA samples. The fluorescence images (Figure 1b) were acquired by exciting the written structures with an LED light source with wavelength (λ_{exc}) of 473 nm and intensity (I_{exc}) of 2 MW/m^2 that is very low compared to the I_{dlw}. The fabricated structures exhibit bright fluorescence as compared to the regions that were unexposed to the writing beam (Figure 1b). The large difference in the fluorescence intensities is attributed to the stabilization of fluorescent silver nanoclusters induced by DLW. Figure 1c shows the intensity profile of the fluorescence across the line array (see marked line in Figure 1b) with an average line breadth of 540 nm.

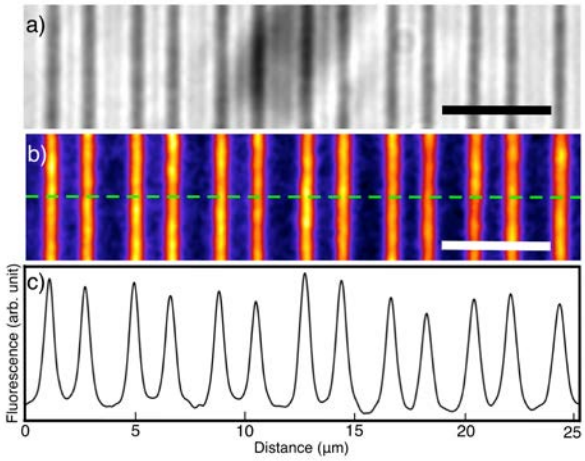

Figure 1. (a) Bright field microscopy image of a fabricated line array in 50% Ag@PMAA samples (I_{dlw} = 80 GW/m^2, λ_{dlw} = 780 nm). Scale bars = 5 μm. (b) Corresponding fluorescence images of the same area (λ_{exc} = 473 nm). (c) Fluorescence intensity profile across the marked line in (b).

Fluorescence obtained from written structures depends on silver concentration. To investigate the origin of the fluorescence emanating from the fabricated structures in the silver-containing polymers, we performed DLW (I_{dlw} = 480 GW/m^2) on samples with different Ag:MAA ratios (0 to 600%). For PMAA films without silver, this laser intensity (I_{dlw} = 480 GW/m^2) did not cause any observable changes to the film, therefore, we used an

I_{dlw} of 880 GW/m^2 to obtain a comparable reference sample (with I_{dlw} of 640 GW/m^2 as threshold). The fluorescence emission spectra were recorded by exciting the region containing written structures using a laser (λ_{exc} = 473 nm) operating at I_{exc} of ~ 2 MW/m^2. In all measurements, the weak fluorescence signal originating from the glass substrate was subtracted. As seen in Figure 2, the fluorescence increases with silver content indicating that the signal is caused by silver nanoclusters in the PMAA matrix. Although structures written on the samples having Ag:MAA ratios of 100%−600% ratios were also fluorescent, these samples were not studied due to unwanted crystallization. Furthermore, addition of silver beyond 75 % Ag:MAA ratio did not further enhance the fluorescence emission intensity (Supporting Information, Figure S1).

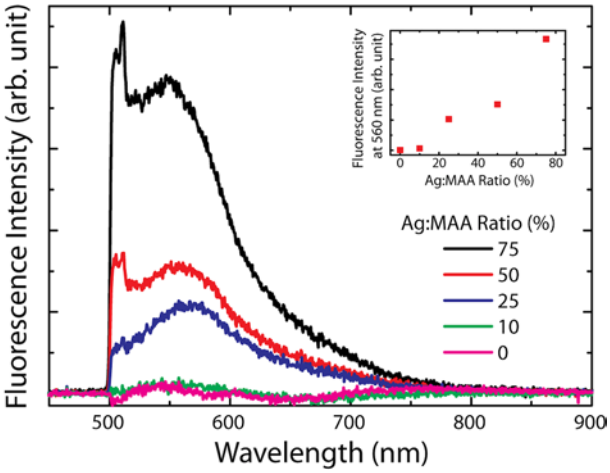

Figure 2. Fluorescence emission spectra of laser-written silver nanoclusters in Ag@PMAA films with Ag:MAA ratios ranging from 0 to 75 % (λ_{exc} = 473 nm). Inset shows the Ag concentration dependence of the fluorescence intensity at 560 nm in Ag@PMAA samples

AFM characterization shows the formation of grooves in the written structures. We used atomic force microscopy (AFM) to perform detailed analysis of the structures written on Ag@PMAA films. Figure 3 shows the AFM images of the structures formed at different I_{dlw} and the corresponding line profiles across the marked regions. Surprisingly, the line profiles revealed the formation of 3D grooves at the location of the laser-written structures. The depths and breadths of the grooves were extracted and averaged from 24 line profiles for each laser

intensity. Correspondingly, the breadths of the grooves written at I_{dlw}= 80, 240, and 480 GW/m^2 were found to be 380 ± 40, 710 ± 120, and 850 ± 80 nm, respectively. The depth of the grooves was measured to be 38 ± 1 nm for all cases while the thickness of the Ag@PMAA film was evaluated as 38 ± 3 nm. Thus, the laser beam ablates most of the material at the exposed regions (Figure 3). The line profiles also show sharp edges of the grooves suggesting the absence of material aggregation as reported in DLW of microstructures in silver-containing luminescent glass.[16,17] Interestingly, despite the fact that most material is ablated under the writing beam, the fluorescence signal is observed precisely at the location of the written structures.

We used scanning electron microscopy with energy dispersive X-ray spectroscopy (SEM-EDS) to determine the presence of silver at the ablated regions of the Ag@PMAA sample. EDS line profiles perpendicular to the written fluorescent lines show a similar level of Ag at written lines as well as at unexposed areas indicating a constant distribution of Ag in the film (Supporting Information, Figure S2). This confirms that the fluorescence signal originating from the written structures is due to the presence of silver despite the ablation.

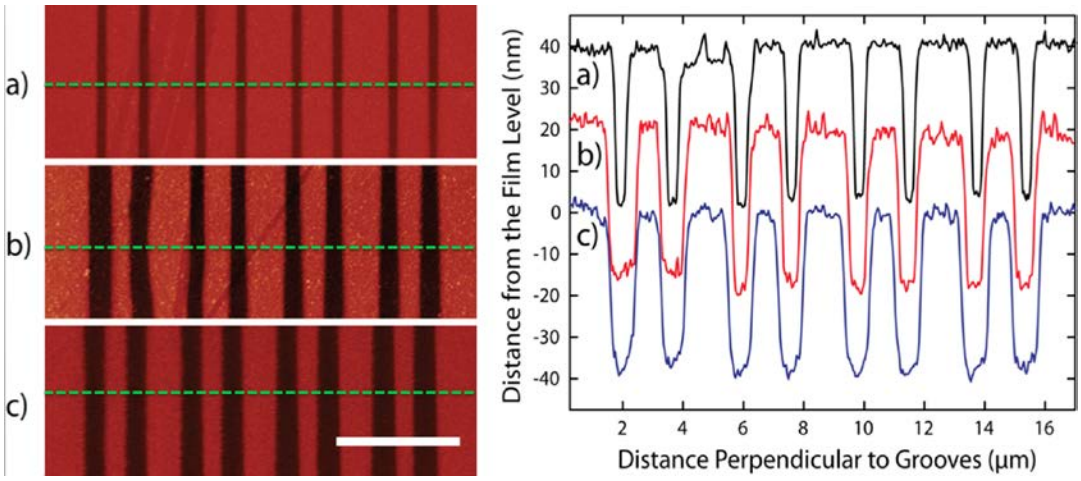

Figure 3. AFM images of structures written with I_{dlw} of (a) 80 GW/m^2, (b) 240 GW/m^2 and (c) 480 GW/m^2 in 50 % Ag@PMAA samples. Scale bar = 5 μm. The full width at half maxima (FWHM) of the grooves measured from line-cut topography profiles (right) are (a) 380 ± 40 nm, (b) 710 ± 120 nm, and (c) 850 ± 80 nm, respectively. For clarity, the line profiles for (a) and (b) have been vertically shifted for 40 and 20 nm, respectively.

The breadth of lines and fluorescence obtained from the written structures increase with laser power. By adjusting writing parameters such as laser intensity and exposure time, *i.e.*, scanning speed, the fluorescence intensity of the fabricated structures can be controlled. Figure 4 shows the fluorescence emission spectra that are obtained from the structures written with different I_{dlw}. As expected, the fluorescence is highest in the structure written with the highest I_{dlw}. Close inspection of the fluorescence images of the written structures further reveals an increase in the breadth of the lines with I_{dlw} (Figure 4, inset). It is worth noting that a steady fluorescence signal coming from the entire breadth of the written lines is observed regardless of the writing laser intensity. Since the transverse spatial resolution of the microscope (~200 nm) is better than the breadths of the written lines (400-900 nm), our observations suggest that the fluorescence originates from nanoclusters at the bottom of the grooves where most of the material is removed. This result is consistent with our SEM-EDS analysis.

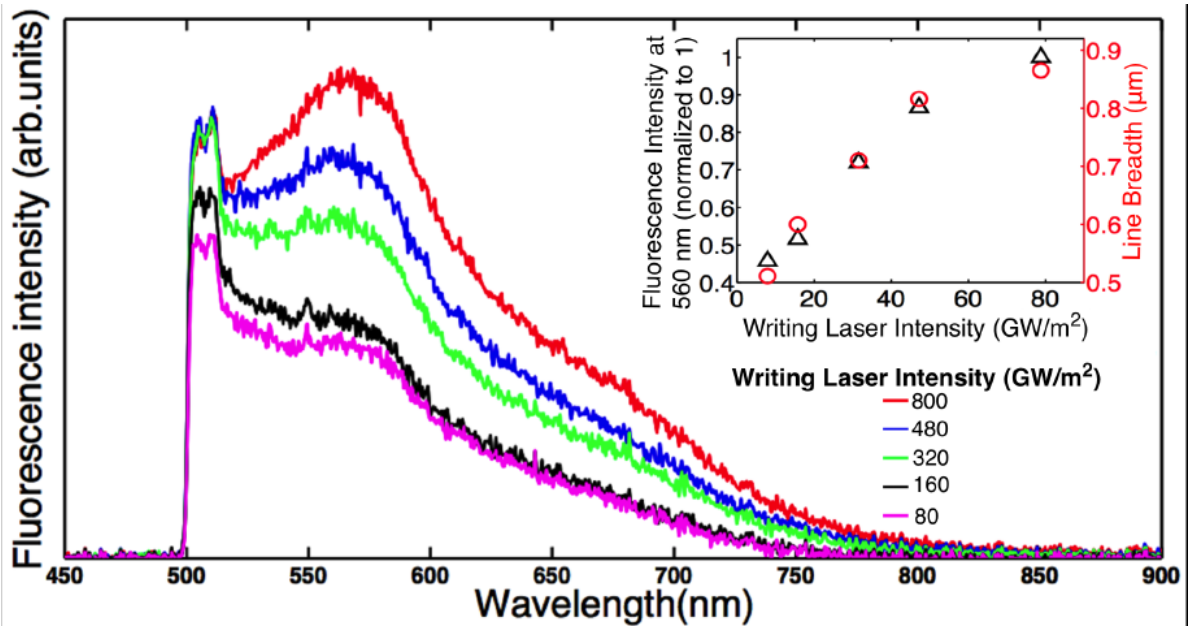

Figure 4. Fluorescence emission spectra (λ_{exc} = 473 nm) recorded from the structures written at different I_{dlw}: 80, 160, 320, 480 and 800 GW/m^2. Inset shows the fluorescence intensity at 560 nm and the corresponding breadth of the fluorescent grooves against writing power.

Optical properties of nanoclusters are similar in character to those observed in solution. To further investigate the optical properties of nanoclusters, we analyzed the fluorescence excitation and emission spectra of the DLW-fabricated microstructures (Figure 5). The written structures show fluorescence emission when excited with wavelengths ranging from 420 nm to 520 nm, with an excitation maximum at 470 nm. Correspondingly, when excited with 473 nm, the written structure shows a broadband fluorescence emission at 500 to 850 nm, with a peak at around 560 nm. Based on the position and the shape of the emission spectrum, we consider that the silver nanoclusters are similar in character to those observed in solution.[12,13]

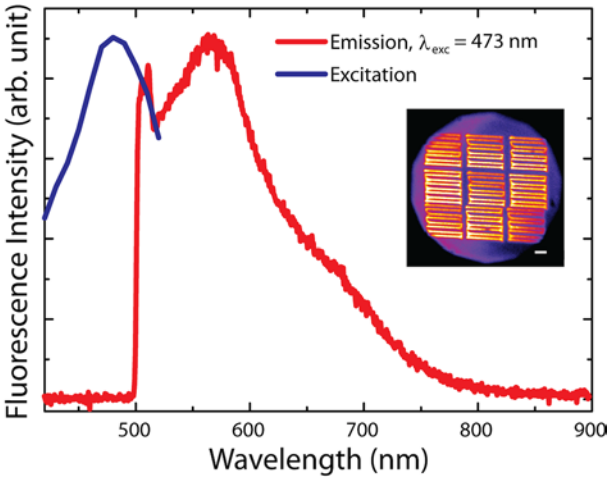

Figure 5. Excitation (blue curve) and emission (red curve) spectra (λ_{exc} = 473 nm) obtained from fluorescent silver nanoclusters in microstructures (inset). Scale bar = 5 µm. The excitation spectrum was measured by evaluating the total emission counts between 532 nm and 650 nm. Inset shows the fluorescence image of the investigated microstructures.

The emission spectrum from the written structures also exhibits a sharp peak at around 510 nm. We suspect that this peak is related to an enhanced Raman scattering effect, whereas the apparent cut-off of the spectrum at shorter wavelengths results from the 500 nm long-pass filter used to avoid unwanted excitation light. To investigate the suspected Raman peak, we measured the Raman spectra from the Ag@PMAA thin films (Figure 6a). The Raman spectrum of the unexposed area does not show any observable signal, whereas the written structures show two broad peaks at 1340 and 1590 cm^{-1}, corresponding to ν_{COO^-} (sym.) and

ν_{COO-} (asym.) vibrations, respectively.[26] The lines observed in the Raman microscopy images of the written structures (Figure 6b) coincide well with the lines in the corresponding brightfield microscopy image (Figure 6c), strongly suggesting that Raman signals are highly localized at the written structures.

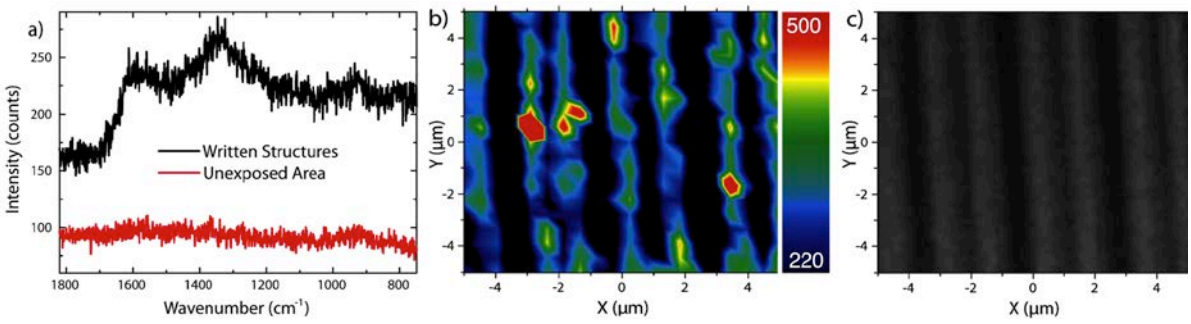

Figure 6. Raman spectra (a) detected from the written structures (black curve) and unexposed regions (red curve). (b) Raman microscopy imaging of the written structures at 1340 cm^{-1}. Color scale bar corresponds to the Raman signal counts. (c) Bright field microscopy image of the corresponding area.

In addition, we measured the emission spectra of the fluorescent structures with a 473 nm LED (I_{exc} of 1 MW/m^2) and a 473 nm diode laser (I_{exc} of 1 MW/m^2) (Figure S4). The emission spectrum recorded with the 473 nm LED does not show a peak at 510 nm, further supporting our claim of the enhanced Raman signal detection. In addition, we found that the peaks obtained by exciting the written structures with 473 nm laser and 532 nm diode laser overlap at the same Raman shift range (1300−1700 cm^{-1}) from the excitation wavelength, thus coinciding with the observed broad Raman signals (Figure S5). Essentially, our observations suggest that nanoclusters interact with the encapsulating polymer through a charge transfer mechanism to enhance the Raman signal as reported in earlier work.[27] Furthermore, as the nanoclusters are too small to support collective electron oscillations, we can disregard plasmonic enhancement effects.

Stabilized nanoclusters show excellent photostability. We also studied in detail the photobleaching of the silver nanoclusters (Figure 7). In general, fluorescence was detected in three parts of the sample: written structures (or areas which are exposed to the writing beam),

unexposed areas of the Ag@PMAA film (background), and glass (substrate). Indeed, in addition to the written structures, fluorescence was also detected in the sample area that was unexposed to the writing beam (Figure 7). The origin of fluorescence in the unexposed area is most likely caused by the generation of nanoclusters in the solution during sample preparation.[28] It is possible that such nanoclusters become kinetically trapped in the film during spin coating and are thus not properly protected by the MAA units, and therefore, produce a fluorescence signal that is highly unstable to illumination. The fluorescence from the glass was found to be weak and was subtracted from the emission data.

The bleaching data were recorded from two distinct areas: from an area unexposed to the writing beam and from an area containing written structures. The area containing written structures includes area exposed to as well as area unexposed to the writing beam (Figure 5 inset). Additionally, bleaching of a Rhodamine 6G reference sample was tested. These data were recorded at two-second intervals for 40 seconds while continuously irradiating the sample with an intensity ~ 0.3 MW/m^2 (λ_{exc} = 473 nm laser diode). The total fluorescence intensity is calculated by integrating the area under the emission spectrum. The bleaching data were normalized and plotted as a function of time (Figure 7). Initially, the fluorescence intensities recorded from the area unexposed to the writing beam and from the area containing the written structures are about at the same level, thus no extra fluorescence was induced by DLW. However, under continuous irradiation the area containing written structures bleaches significantly slower than the area unexposed to the writing beam. This suggests that DLW stabilizes the existing nanoclusters rather than that it creates new ones.

Furthermore, Figure 7 shows that the fluorescence obtained from the unexposed area bleaches to approximately 10% of its initial value within 20 seconds. The bleaching curve obtained from this unexposed area can be fitted by a single exponential decay equation y=a*exp(-t/τ_1)+c, with a bleaching time constant (τ_1) of 4.3 s, where a, t, and c are amplitude,

time and offset parameters, respectively. On the other hand, the fluorescence bleaching curve of the area containing written structures can be fitted accurately by a double exponential decay equation y=a*exp(-t/τ_1)+b*exp(-t/τ_2) with bleaching time constants τ_1 and τ_2 of 4.7 s and 350 s, respectively. Table 1 summarizes the bleaching time constants resulting from the fitting. The bleaching time constant τ_1 has almost the same value in both of the fits, and therefore, the fast-decaying τ_1 is assigned to the bleaching of the area unexposed to the writing beam. The time constant τ_2 is associated with the bleaching of the fluorescence originating from the area exposed to the writing beam, *i.e.*, the written structures. The fluorescence from the written structures is highly photostable having the bleaching time constant of 350 s.

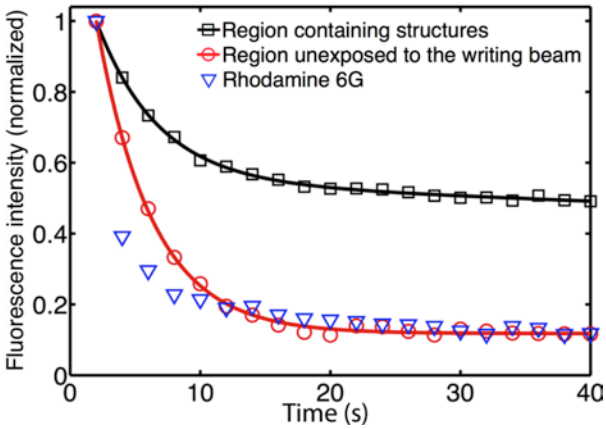

Figure 7. Photobleaching curves of area containing written structures, area unexposed to writing beam and Rhodamine 6G dye. The microstructures were written with I_{dlw} = 480 GW/m^2 (λ_{dlw} = 780 nm) in 50% Ag@MAA film. The bleaching was induced by irradiating the samples with a laser (λ_{exc} = 473 nm, I_{exc} = 0.3 MW/m^2). The solid lines represent single exponential and biexponential fits to the data points respectively from the area unexposed to writing beam and from area containing written structures.

Table 1. Comparison of bleaching time constant of written structures and background.

	bleaching time constant of background (τ_1)	bleaching time constant of written structure (τ_2)
Area Containing Structures	4.7 s	350 s
Area Unexposed to Writing Beam	4.3 s	---

We also compared the photostability of $(Ag)_n$@PMAA nanoclusters against the conventional fluorescent dye, Rhodamine 6G. The fluorescence of the dye bleaches even faster than the Ag@PMAA film background under identical experimental conditions, thus showing the high photostability of the written structures (Figure 7). This observation agrees with earlier studies on the photostability of silver nanoclusters in other scaffolds, such as glass,[16,17] zeolites[18] and DNA.[8] It is worth noting, that the fluorescence images (Figure 1) and spectra (Figures 2, 4 and 5) were recorded with I_{exc} of 2 MW/m^2. Already such low laser intensity bleaches the unexposed Ag@PMAA background within a second, leaving the written structures as the main source of fluorescence in these experiments.

CONCLUSIONS

We have demonstrated the DLW of fluorescent microstructures by stabilizing silver nanoclusters in silver-containing PMAA films. Fluorescent structures were written by a tightly focused near-infrared femtosecond laser beam, thereby reaching line breadths of submicron scale. To the best of our knowledge, this is the first report about the DLW of fluorescent silver nanoclusters in an organic matrix. The formed nanoclusters are highly photostable. This fabrication method could open new opportunities in nanophotonics applications like imaging, labeling, and metal ion sensing. Furthermore, we anticipate the

applicability of our technique in the synthesis of similar metal nanoclusters that are embedded in relevant polymer matrices.

METHODS

Sample preparation. Silver-containing thin films of PMAA (Ag@PMAA) were prepared by spin coating. Aqueous solutions of PMAA (PolySciences, M_w = 100 000 g/mol) and $AgNO_3$ (Sigma-Aldrich, > 99.8 %) were mixed to obtain a PMAA concentration of 1.5 wt% and Ag:MAA ratios ranging from 0 to 600 %, *e.g.*, a ratio of 50 % corresponded to one Ag^+ ion per two MAA units. Before spin coating, the borosilicate glass substrates (22 mm × 22 mm × 0.19 mm) were cleaned by rinsing with ethanol and water and dried with nitrogen. The thin films were spin coated on the substrates at 1500 RPM for 120 s. Subsequently, the films were dried in vacuum for 12 h. The water used throughout experiments was Milli-Q grade with a resistivity of 18.2 MΩ·cm.

Direct laser writing. The DLW setup (Supporting Information, Figure S7) was employed to fabricate 2D structures in Ag@PMAA samples. A pulsed laser beam (780 nm, 80 MHz, 290 fs) was directed and focused by a microscope objective lens (100×, NA = 1.4, oil, Leica) onto the sample that is mounted on a 3D nanopositioner. In order to write the structures, the samples were scanned with a speed of 10 μm/s over a fixed laser beam with a regulated input power (P = 5−50 mW corresponding to illumination intensities of 80−800 GW/m^2). The focused writing laser spot size was 284 nm in diameter, estimated by the formula, spot size = 0.51*λ_{dlw}/NA, where λ_{dlw} is wavelength of laser beam and NA is numerical aperture of objective lens. Samples with Ag:MAA ratio over 75 % were neglected due to severe crystallization observed in those samples (see Supporting Information, Figure S1). An incorporated brightfield microscopy imaging arm was used to monitor the fabrication of the structures.

AFM and SEM characterization. The thickness of Ag@PMAA films was determined by atomic force microscopy (AFM) in tapping mode (Veeco Dimension 5000 AFM with Nanoscope V controller). The film was scratched with a scalpel and the AFM tip (HQ:NSC15/Al BS, MikroMasch) was scanned perpendicular to the scratch. In addition, AFM was used for detailed characterization of the topographical features of the samples. Field-emission scanning electron microscopy was performed at 1.5 keV electron energy (JEOL JSM-7500FA). The $(Ag)_n$@PMAA thin film sample was coated with thin layer of carbon prior to measurements (Emitech K950) to promote sample conductivity. Energy-dispersive X-ray analysis was performed with the JSM-7500FA using a Be thin film window and liquid nitrogen cooled detector. Line spectra across DLW written structures were recorded using 10 keV electron energy to analyze the composition of samples.

Optical characterization. The optical properties of the fabricated structures were characterized using a custom-built fluorescence microscope (Supporting Information, Figure S8). The fluorescence emission spectra were recorded from a set of laser written line array structures using a spectrometer and the excitation spectrum was measured using a photomultiplier tube (see Supporting Information for details). The fluorescence images were colored according to their greyscale values with ImageJ software. Absorption spectra of the thin films were recorded in the UV−visible range with PerkinElmer Lambda 950 UV/Vis/NIR absorption spectrometer. Raman scattering measurements were carried out with a Horiba Jobin-Yvon Labram HR 300 using 785 nm IR diode laser excitation source with 100x air objective (laser spot diameter < 1 μm). Raman mapping was performed by measuring 20x20 point spectra from 5x5 μm area. The laser intensity in Raman measurements was kept low compared to DLW writing intensity.

ASSOCIATED CONTENT

Supporting Information. Detailed description of experimental setups, measurements and additional data. This material is available free of charge via the Internet at http://pubs.acs.org.

AUTHOR INFORMATION

Corresponding Author

juha.toivonen@tut.fi

robin.ras@aalto.fi

Author contributions

P. K. and J. H. contributed equally to this work.

ACKNOWLEDGMENT

This work was supported by the Academy of Finland through its Centres of Excellence Programme (2014-2019) and under Projects No. 135043, 135201, 267847, 135159 and 256314. P.K. acknowledges support from the Graduate School of Tampere University of Technology. This work made use of the Aalto University Nanomicroscopy Center (Aalto-NMC) premises. This work was performed in the context of the European COST Action MP1302 Nanospectroscopy.

REFERENCES

1. Zheng, J; Nicovich, P. R.; Dickson, R. M. Highly Fluorescent Noble Metal Quantum Dots. *Annu. Rev. Phys. Chem.* **2007**, *58*, 409–431.
2. Díez, I.; Ras, R. H. A. Fluorescent Silver Nanoclusters. *Nanoscale* **2011**, *3*, 1963.
3. Wilcoxon, J. P.; Abrams, B. L. Synthesis, Structure and Properties of Metal Nanoclusters. *Chem. Soc. Rev.* **2006**, *35*, 1162−1194.
4. Shang, L.; Dong, S.; Nienhaus, G. U. Ultra-Small Fluorescent Metal Nanoclusters: Synthesis and Biological Applications. *Nano Today* **2011**, *6*, 401−418.
5. Peyser, L. A.; Vinson, A. E.; Bartko, A. P.; Dickson, R. M. Photoactivated Fluorescence from Individual Silver Nanoclusters. *Science* **2001**, *103*, 103−106.
6. Díez, I.; Ras, R. H. A.; Kanyuk, M. I.; Demchenko, A. P. On Heterogeneity in Fluorescent Few-Atom Silver Nanoclusters. *Phys. Chem. Chem. Phys.* **2013**, *15*, 979−985.

7. Chakraborty, I.; Govindarajan, A.; Erusappan, J.; Ghosh, A.; Pradeep, T.; Yoon, B.; Whetten, R. L.; Landman, U. The Superstable 25 kDa Monolayer Protected Silver Nanoparticle: Measurements and Interpretation as an Icosahedral $Ag_{152}(SCH_2CH_2Ph)_{60}$ Cluster. *Nano Lett*. **2012**, 12, 5861–5866.
8. Petty, J. T.; Story, S. P.; Hsiang, J.-C.; Dickson, R. M. DNA-Templated Molecular Silver Fluorophores. *J. Phys. Chem. Lett*. **2013**, *4*, 1148–1155.
9. Gonzáles, B. S.; Blanco, M. C.; López-Quintela, A. DNA-Templated Molecular Silver Fluorophores. *Nanoscale* **2012**, 4, 7632−7635.
10. Ershov, B. G.; Henglein, A. Reduction of Ag+ on Polyacrylate Chains in Aqueous Solution. *J. Phys. Chem. B* **1998**, 102, 10663−10666.
11. Zhang, J.; Xu, S.; Kumacheva, E. Photogeneration of Fluorescent Silver Nanoclusters in Polymer Microgels. *Adv. Mater*. **2005**, *17*, 2336–2340.
12. Shang, L.; Dong, S. Facile Preparation of Water-Soluble Fluorescent Silver Nanoclusters Using a Polyelectrolyte Template. *Chem. Commun*. **2008**, 1088−1090.
13. Díez, I.; Pusa, M.; Kulmala, S.; Jiang, H.; Walther, A.; Goldmann, A. S.; Müller, A. H. E.; Ikkala, O.; Ras, R. H. A. Color Tunability and Electrochemiluminescence of Silver Nanoclusters. *Angew. Chem. Int. Ed*. **2009**, *48*, 2122–2125.
14. Rongqing, L.; Wang, C.; Bo, F.; Wang, Z.; Shao, H.; Xu, S.; Cui, Y. Microwave-Assisted Synthesis of Fluorescent Ag Nanoclusters in Aqueous Solution. *ChemPhysChem* **2012**, *13*, 2097−2101.
15. Xu, H.; Suslick, K. S. Sonochemical Synthesis of Highly Fluorescent Ag Nanoclusters. *ACS Nano* **2010**, *4*, 3209−3214.
16. Bellec, M.; Royon A.; Bourhis, K.; Choi, J.; Bousquet, B.; Treguer, M.; Cardinal, T.; Videau, J.-J.; Richardson, M.; Canioni, L. 3D Patterning at the Nanoscale of Fluorescent Emitters in Glass. *J. Phys. Chem. C* **2010**, *114*, 15584–15588.
17. Royon, A.; Bourhis, K.; Bellec, M.; Papon, G.; Bousquet, B.; Deshayes, Y.; Cardinal, T.; Canioni, L. Silver Clusters Embedded in Glass as a Perennial High Capacity Optical Recording Medium. *Adv. Mater.* **2010**, *22*, 5282−5286.
18. De Cremer, G. D.; Sels B. F.; Hotta J.; Roeffaers, M. B. J.; Bartholomeeusen, E.; Coutino-Gonzales, E.; Valtchev, V.; De Vos, D. E.; Vosch, T.; Hofkens, J. Optical Encoding of Silver Zeolite Microcarriers. *Adv. Mater.* **2010**, *22*, 957–960.
19. Zewail, A. Femtochemistry: Atomic-Scale Dynamics of the Chemical Bond Using Ultrafast Lasers. *Angew. Chem*. **2000**, 39, 2587-2631.
20. Zhang, Y.; Chena, Q.; Xia, H.; Sun, H. Designable 3D Nanofabrication by Femtosecond Laser Direct Writing. *Nano today*. **2010**, 5, 435-448.
21. Farsari, M.; Chichkov B. N. Two-Photon Fabrication. *Nat. Photon*. **2009**, *3*, 450–452.
22. Kawata, S.; Sung, H.; Tanaka, T.; & Takada, K. Finer Features for Functional Microdevices. *Nature* **2001**, 412, 697−698.
23. Sun, H. B.; Kawata, S. Two-Photon Photopolymerization and 3D Lithographic Microfabrication. *Adv. Polym. Sci.* **2004**, *170*, 169−273.
24. Park, J.-J.; Prabhakaran, P.; Jang, K. K.; Lee, Y.; Lee, J.; Lee, K.; Hur, J.; Kim, J.-M.; Cho, N.; Son, Y. et al. Photopatternable Quantum Dots Forming Quasi-Ordered Arrays. *Nano Lett.* **2010**, *10*, 2310−2317.

25. Stellacci, F.; Bauer, C. A.; Meyer-Friedrichsen, T.; Wenseleers, W.; Alain, V.; Kuebler, S. M.; Pond, S. J. K.; Zhang, Y.; Marder, S. R.; Perry, J. W. Laser and Electron-beam Induced Growth of Nanoparticles for 2D and 3D Metal Patterning. *Adv. Mater.* **2002**, *14*, 194−198.
26. Socrates, G. *Infrared and Raman Characteristic Group Frequencies*; John Wiley & Sons Ltd: Chichester, 2001; p 128.
27. Peyser-Capadona, L.; Zheng, J.; González, J. I.; Lee, T.-H.; Patel, S. A.; Dickson, R. M. Nanoparticle-Free Single Molecule Anti-Stokes Raman Spectroscopy. *Phys. Rev. Lett.* **2005**, 058301.
28. Xiong, Y.; Washio I.; Chen J.; Sadilek M.; Xia Y. Trimeric Clusters of Silver in Aqueous $AgNO_3$ Solutions and Their Role as Nuclei in Forming Triangular Nanoplates of Silver. *Angew. Chem. Int. Ed*. **2007**, 46, 4917−4921.